SISSA

A robust large area x-ray imaging system based on 100 μ m thick Gas Electron Multiplier

To cite this article: F.D. Amaro *et al* 2015 *JINST* **10** C12005

View the article online for updates and enhancements.

IOP ebooks™

Bringing you innovative digital publishing with leading voices to create your essential collection of books in STEM research.

Start exploring the collection - download the first chapter of every title for free.

A robust large area x-ray imaging system based on 100 μm thick Gas Electron Multiplier

F.D. Amaro,[a] **J.A. Mir,**[a] **X. Carvalho,**[a] **C.D.R. Azevedo,**[b] **J.M.F. dos Santos**[a,1] **and H. Natal da Luz**[c]

[a]*LIBPhys, Department of Physics, University of Coimbra,*
  Rua Larga, PT3004-516 Coimbra, Portugal

[b]*I3N, Department of Physics, University of Aveiro,*
  Campus UniversitÃqrio de Santiago, 3810-193, Aveiro, Portugal

[c]*Instituto de FÃηsica, Universidade de SÃčo Paulo,*
  Rua do MatÃčo, 05508-090 Cidade UniversitÃqria, SÃčo Paulo, Brasil

  E-mail: jmf@gian.fis.uc.pt

ABSTRACT: We have developed an imaging detector based on a non-standard GEM, made from a 100 μm thick kapton foil (2-fold thicker than standard GEM's). The 100 micron thick GEM is produced using the same wet etching technique as the standard GEM and is less prone to the damage caused by discharges, creating a robust detector that can safely operate at high gain.

In this work we present the results obtained with a cascaded gaseous electron multiplier composed by two 100 micron thick GEM and a 10×10 cm^2 bi-dimensional readout electrode with resistive charge division. We have recorded energy resolution of 21% and charge gains above 10^4 when the detector was irradiated with 5.9 keV X-rays emitted by a ^{55}Fe radioactive source. We also present 10×10 cm^2 images acquired with the detector when irradiated with X-rays. The minimum position resolution recorded was 1.7 mm.

---

[1]Corresponding author.

Contents

1 Introduction

Most of the imaging applications with Gas Electron Multipliers (GEM) [1] as amplification devices traditionally make use of discrete channel readout. These solutions provide excellent spatial resolution (of the order of hundreds of μm) for areas as large as $10 \times 10 \, \text{cm}^2$. However they require a large number of complex and expensive electronic channels [2]. For applications where spatial resolutions in the order of the mm are required, a simpler and cheaper solution is to determine the position of the interaction using resistive charge division [3]. This solution greatly simplifies the electronic system, since it requires a minimum number of only 4 readout channels to achieve 2D imaging over large areas. It is however very much dependent on obtaining a high signal-to-noise ratio. This means that the GEM's must be operated at high gain and, in some cases, near the discharge limit. The consequence of operating at such a regime is the higher discharge probability and as consequence, the higher detector damage probability.

We have developed a non-standard GEM, made from a $100 \, \mu$m thick kapton foil (2-fold thicker than standard GEM's). The $100 \, \mu$m GEM were produced at CERN with an active area of $10 \times 10 \, \text{cm}^2$, using the same wet etching technique as the standard GEM. A gaseous electron multiplier composed by two 100 micron GEM elements cascaded with a bi-dimensional readout was already fully characterized in the past [4], presenting the necessary signal-to-noise ratio for imaging applications. The bi-dimensional readout used in [4] had an active area of only $5 \times 5 \, \text{cm}^2$.

In this work we present the results achieved with a gaseous electron multiplier, composed by a cascade of two $100 \, \mu$m GEM coupled to a $10 \times 10 \, \text{cm}^2$ bi-dimensional readout.

2 Experimental setup

A schematic representation of the detector used in this work is presented in figure 1. It is composed by an absorption/drift region followed by a cascade of two $100 \, \mu$m thick GEM. The final avalanche charge is extracted from the last GEM of the cascade and collected by a 2D resistive readout. The drift region, 9 mm deep, is limited by the drift electrode (a stainless steel mesh made of $80 \, \mu$m

diameter wires with 900 μm spacing) and the top electrode of the first GEM in the cascade. The transfer and induction regions were respectively 3 and 6 mm deep. The GEM foils, the drift electrode and the 2D readout had an area of $10 \times 10\,\text{cm}^2$. The cascaded electron multiplier was immersed in a mixture of argon (70%):CO_2(30%) at atmospheric pressure. The gas mixture was continuously flowing through the detector at a flow rate of 5 l/h, supplied from an adjacent pressurized canister. The entrance window of the chamber was made by a aluminized Mylar™ film with a thickness of 25 μm.
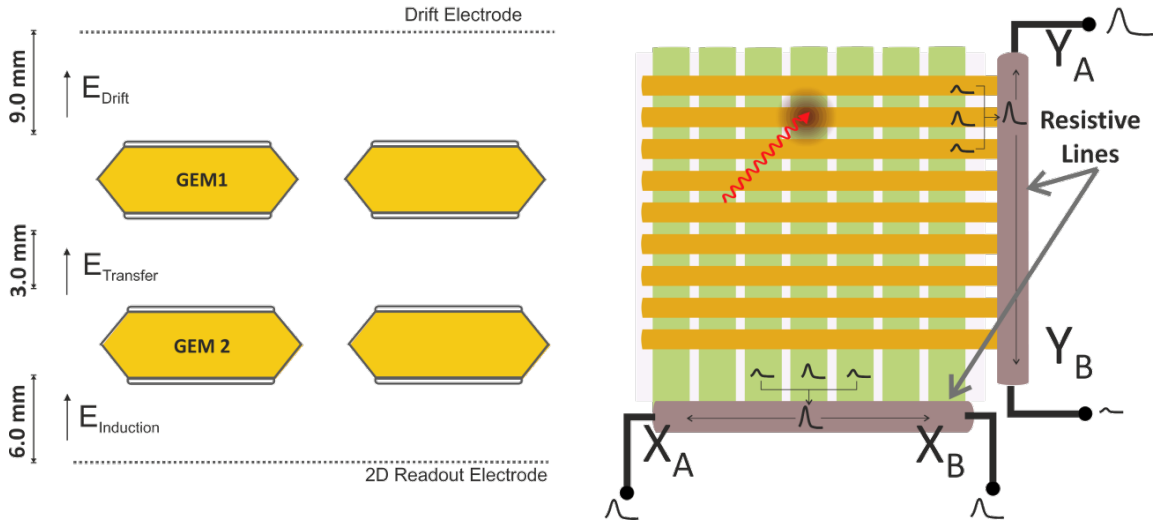
Figure 1. Schematics of the detector (left) and of the 2D resistive readout (right) used in this work. The detector is a cascade of two 100 μm thick GEM. A metallic mesh limits the drift region (9.0 mm deep) and a 2D resistive readout is used to collect the final charge extracted from the holes of GEM 2.

Each of the detector electrodes was independently biased with a CAEN V6521HN power supply. The readout electrode was at ground potential and the other electrodes were polarized with negative voltages.

The charge readout electrode, with an area of $10 \times 10\,\text{cm}^2$, was composed by two layers of parallel strips with 200 μm pitch. The two layers were rotated by 90° with respect to each other and separated by an insulating layer. The areas of the strips of each layer were adjusted so that the charge is equally shared between the layers. The strips of each layer were interconnected by a resistive line ($\sim 5\,\text{k}\Omega$) and the signals were collected from both ends of the resistive line. The ratio between the amounts of charge reaching each end of the resistive line has information of the position of interaction for the corresponding dimension. This technique provides information of the position and energy of each event produced in detector, making use of only four shaping/amplification channels. The position along each dimension is given by:

$$y = L\frac{Y_L - Y_R}{Y_L + Y_R} \tag{2.1}$$

Where the y is the position along one of the dimensions, Y_L and Y_R are the amplitude of the signals collected at each end of the resistive line and L is the length of the line. The energy information was obtained by summing the contributions from both resistive lines.

The charge pulses collected at each of the four channels, were integrated by a charge sensitive preamplifier with a rise time of 100 ns, and digitized by a CAEN VME1728 digital pulse processor, where the time shaping and amplification was done in real time by the built-in FPGA by applying the Jordanov algorithm [5]. The amplitude and the time stamp, with a resolution of 10 ns, of each pulse were recorded in all the four electronic channels. In the first step of the data processing, the information on each of these 4 channels was compared and the pulses were organized into events. Each event was composed by four pulses, one from each channel, occurring within a time window of a few ns. Whenever this condition was not met, the pulses were discarded and no event was reconstructed. The output of this first step was a collection of events with position (x and y) energy (E) and time information (t).

An X-ray tube, equipped with a copper anode, was placed at a distance of about 2 m from the detector window and used to irradiate several masks of stainless steel or lead. The X-ray beam was filtered with a 1.5 mm aluminum foil.

3 Results

3.1 Gain and energy resolution mapping

Prior to the image acquisition with the x-ray tube we have irradiated our detector, point-by-point, using x-rays emitted from a ^{55}Fe radioactive source. Irradiation points were located in a 10×10 matrix, with a separation of 1 cm between each point. The source was collimated to 4 mm diameter. For this study we have interconnected the 4 output channels of the 2D resistive electrode readout and the resulting avalanche charge was collected by a Canberra 2006 charge sensitive pre-amplifier. The output signal was then fed to a Tennelec TC 243 linear amplifier (4 μs shaping time) and a Nucleus PCA 2 multichannel analyser. The electronic chain sensitivity was calibrated by injection of a known charge into the preamplifier input.

The electric field in the drift region, transfer and induction region was set to 1.44 kVcm^{-1}, 3.33 kVcm^{-1} and 1.83 kVcm^{-1}, respectively. Voltage difference across GEM$_1$ and GEM$_2$ was set to 580 V. An average energy resolution of 24.7% and a gain of 4.1×10^3 were measured for the 5.9 keV X-rays emitted from the ^{55}Fe radioactive source, over the 10×10 cm^2 of the detector.

Figure 2 presents the results of the detector irradiation. Maximum gain deviation, 10% from the average gain (4.1×10^3), was recorded at the edges of our detector. Energy resolution presented maximum fluctuation of 4.9% with maximum values at the edges of the detector. The lower gains recorded on the central region are most likely related to the resistive lines of the 2D readout: although (for the above measurements) the 4 output channels were short-circuited, each signal propagated along the resistive line. Besides the charge division, the resistive line also attenuates the amplitude and increases the peaking time of the propagating pulses [6]. Events located away from the edges of the active area of the detector suffer more attenuation than the ones at the edges, leading to a slightly lower observable gain. The changes in the peaking time may also account for the energy resolution fluctuations. Nevertheless, following the event position resolution determination, gain correction may be implemented by dividing the 10×10 cm^2 area in a pre-established number of regions (e.g. 1×1 cm^2 regions) and using an established matrix with calibrated correction factors to produce an uniform average gain throughout the full area.

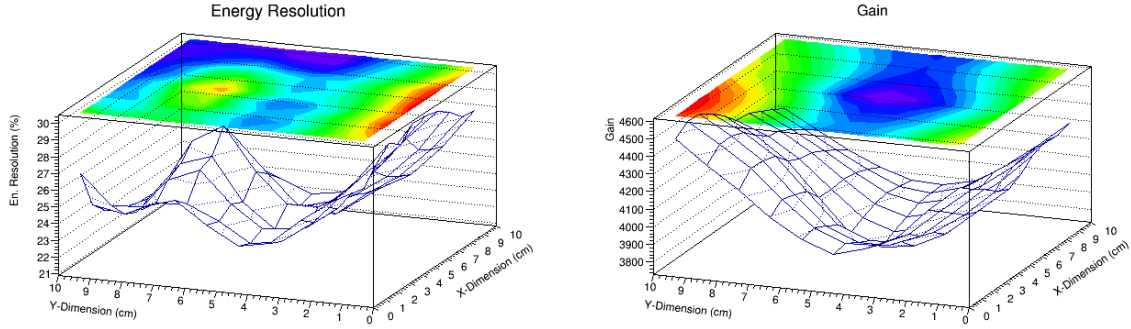**Figure 2**. Gain and Energy resolution map. Detector was irradiated by a ^{55}Fe point source. 100 irradiation points were distributed over a 10×10 matrix, covering the entire $10 \times 10\,\mathrm{cm}^2$ active surface of our detector.

3.2 Imaging

The imaging performance of our apparatus was evaluated by irradiating a series of masks with photons emitted from an x-ray tube equipped with a copper anode. One way to characterize the imaging system is to evaluate the one dimensional Point Spread Function (PSF) of the system. For that, a stainless steel mask with a 1 mm wide slit was imaged using the setup described in the experimental section. This one dimensional approach of the PSF — the Line Spread Function (LSF) — is very convenient, since it is easier to image a thin slit than a very small hole. For calibration of our imaging system purposes, the mask we have irradiated was composed by two 1 mm wide slits, separated by 6 mm. The number of pixels/mm of our system was obtained from the distance between slits in our image.

The profile of our image is plotted on figure 3, superimposed with a Gaussian distribution. The width of the distribution is 1.80 mm. The image of figure 3 is the convolution of the LSF with a 1 mm wide slit. To de-convolute the contribution of the slit from the LSF an empirical equation that approximately determines the width of the LSF as a function of the object and the image widths is used [7]:

$$\sigma_x = \omega_0 \times \sqrt[3]{\left(\frac{\omega_i}{\omega_0}\right)^3 - 1} \tag{3.1}$$

where σ_x is the width of the LSF, ω_0 is the width of the slit (1 mm) and ω_i is the width of the Gaussian distribution fitted to the image in figure 3 (1.8 mm). We have obtained a value of 1.69 mm for σ_x, which represents the minimum width that can be discriminated with the imaging system.

For each reconstructed event, the position along each of the resistive lines (x, y), the time stamp of the event (t) and the energy (E) are recorded. In figure 4 we present the energy distribution of the x-rays used for the image reconstruction of the pair of slits in figure 3.

For each energy band on the spectrum of figure 4, a Gaussian curve was fitted to the projected profile of the slit image. The position resolution, obtained using equation (3.1), is related with the FHWM of the Gaussian curves, depicted on figure 4, as a function of the energy of the x-ray.

The position resolution attainable with the $10 \times 10\,\mathrm{cm}^2$ imaging system is presented on figure 5 as a function of the x-ray energy recorded. For energies up to 15 keV the position resolution is dominated by the SNR. The red curve in the figure shows the expected position resolution as a
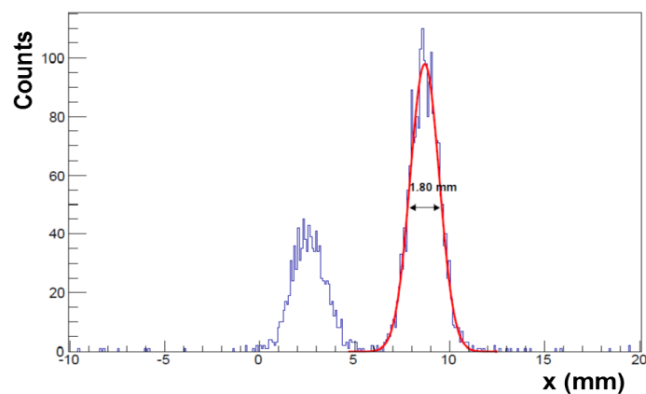
Figure 3. X coordinate projection of the image recorded when a pair of 1 mm wide slits was irradiated with photons emitted by an x-ray tube generator.
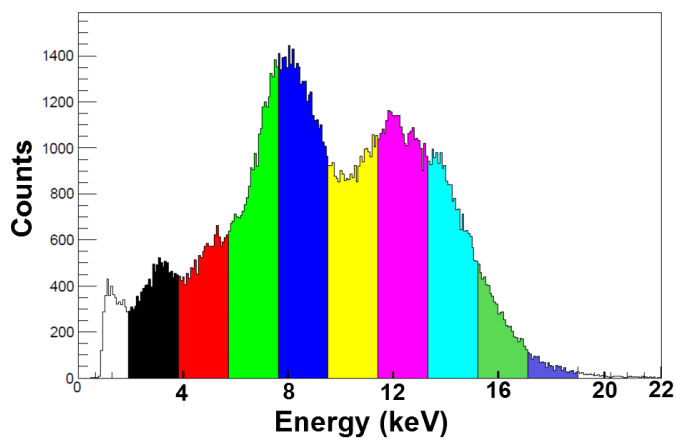

Figure 4. Energy distribution of the x-rays recorded by the imaging system.
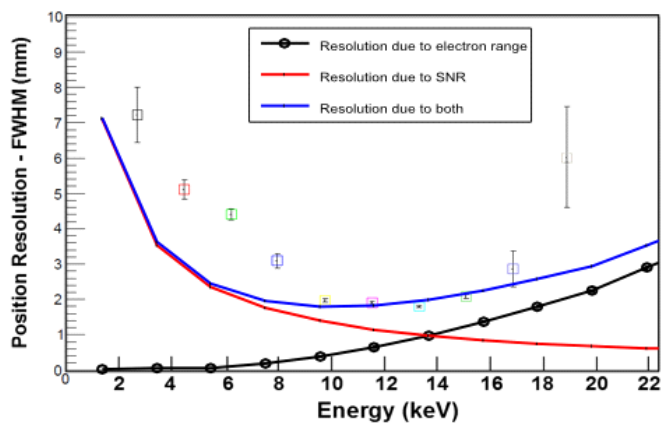

Figure 5. FWHM of the Gaussian curves fitted to the x-projection of the 1 mm slit, as a function of the selected energy band. The curves showing the influence of the signal-to-noise ratio and the photo-electron range are also plotted in red and black, respectively. Details in the text.

function of the signal-to-noise ratio, derived from a model described in [10]. As the number of primary electron produced by the incoming x-ray increases so does the SNR, resulting in an improvement of the position resolution up to the point where the position resolution is dominated by the range of the photo-electron emitted by the argon atom in the $Ar(70\%):CO_2(30\%)$ gas mixture. This range has a direct influence on the position resolution and keeps increasing with the energy of the incoming x-rays. The intrinsic position resolution achievable with the $Ar(70\%):CO_2(30\%)$ gas mixture is plotted in black and was simulated using the software tool Degrad [8] following the procedure described in [9]. The contribution of both factors for the position resolution is described by the blue line in the plot and matches the results obtained for the energies ranging from 9 keV to 17 keV.

4 Conclusions

We have operated a $10 \times 10\,cm^2$ double GEM cascade imaging system composed by only four electronic readout channels. The GEMs are made from a $100\,\mu m$ thick Kapton, producing a robust, spark resistant, gaseous electron multiplier. We have achieved an average charge gain, over the total $100\,cm^2$ area of the detector, of 4.1×10^3 with a maximum deviation of 10%. An energy resolution of 24.7% for 5.9 keV X-rays was recorded with a maximum deviation of 4.9% from the average value.

The imaging performance was evaluated by irradiating the imaging system with photons from an x-ray generator. The minimum position resolution recorded for the $100\,cm^2$ imaging system was 1.69 mm. This figure compares to the one achieved, using the same double $100\,\mu m$ GEM imaging system equipped with a $5 \times 5\,cm^2$ bi-dimensional readout, 1.67 mm [3]. This shows that large area imaging systems using only 4 readout channels can be implemented, without significant performance deterioration.

References

[1] F. Sauli, *GEM: A new concept for electron amplification in gas detectors*, *Nucl. Instrum. Meth.* **A 386** (1997) 531.

[2] J. Brau, M. Breidenbach, A. Dragone, G. Fields, R. Frey, D. Freytag et al., *KPiX — A 1,024 Channel Readout ASIC for the ILC*, *IEEE Nucl. Sci. Symp. Conf. Rec.* (2012) pp. 1857–1860.

[3] H. Natal da Luz, J.F.C.A. Veloso, J.M.F. dos Santos and J.A. Mir, *A simple X-ray position detection system based on a MHSP*, *Nucl. Instrum. Meth.* **A 580** (2007) 1083.

[4] H. Natal da Luz, J.A. Mir, X. Carvalho and J.M.F. dos Santos, *X-ray imaging with GEMs using 100 µm thick foils*, 2014 *JINST* **9** C06007 [arXiv:1311.6862].

[5] V.T. Jordanov, G.F. Knoll, A.C. Huber and J.A. Pantazi, *Digital techniques for real-time pulse shaping in radiation measurements*, *Nucl. Instrum. Meth.* **A 353** (1994) 261.

[6] D. Bassignana, M. Fernandez, R. Jaramillo, M. Lozano, F.J. Muñoz, G. Pellegrini et al., *First investigation of a novel 2D position-sensitive semiconductor detector concept*, 2012 *JINST* **7** P02005 [arXiv:1106.5405].

[7] H. Klein, H. Brede, and B.R.L. Siebert, *Energy and angle straggling effects in a D(d,n)^{3}He neutron source using a gas target*, *Nucl. Instrum. Meth.* **A 193** (1982) 635.

[8] S. Biagi, *Degrad*. Available at: http://consult.cern.ch/writeup/magboltz/.

[9] C.D.R. Azevedo, S. Biagi, R. Veenhof, P.M. Correia, A.L.M. Silva, L.F. N.D. Carramate et al., *Position resolution limits in pure noble gaseous detectors for X-ray energies from 1 to 60 keV*, *Phys. Lett.* **B 741** (2015) 272.

[10] J.P. Cussonneau, M. Labalme, P. Lautridou, L. Luquin, V. Metivier, A. Rahmani et al., 2*D localization using resistive strips associated to the MicrOMEGAs structure*, *Nucl. Instrum. Meth.* **A 492** (2002) 26.